



Effect of nanodiamond reinforcement and heat-treatment on microstructure, mechanical and tribological properties of cold sprayed aluminum coating

Archana Loganathan, Sara Rengifo, Alexander Franco Hernandez, Cheng Zhang,
Arvind Agarwal*

Plasma Forming Laboratory, Department of Mechanical and Materials Engineering, Florida International University, Miami, FL 33174, United States of America



ARTICLE INFO

Keywords:

Nanodiamond (ND)
Cold spray
Heat-treatment
Coefficient of friction
Aluminum

ABSTRACT

Nanodiamond (ND) is a superhard nanoparticle reinforcement for metal matrix composites with its superior hardness and wear properties. A homogeneous dispersed ND aluminum metal matrix composite coating was successfully synthesized by the cold spray process in the present study. TEM investigations of the as-sprayed coating corroborate nanodiamond's uniform distribution, an array of dislocations formed within the Al matrix and along the grain boundaries. A coating density of 99% was achieved upon heat-treatment due to the reduced porosity and good inter-splat bonding. Superhard ND reinforcement in the Al metal matrix coating contributed to a ~96% increase in microhardness compared to pure Al coating, which increased to 135% after heat treatment. The coefficient of friction for heat-treated Al-2 wt% ND coating decreased to ~35%, and the wear rate decreased by ~34% compared to the as-sprayed coating. This study demonstrates that a small (2 wt%) amount of ND addition in the Al matrix inhibits grain growth during heat treatment and increases microhardness and tribological properties.

1. Introduction

There has been a significant volume of research in metal matrix composites (MMCs) due to their potential ability to enhance strength, hardness, thermal conductivity, damping, and wear properties [1–4]. Aluminum-based MMCs (Al-MMC) have been extensively studied due to their lightweight, high strength combination and widely used in automobile, marine, aerospace, and defense applications [5–7]. Aluminum matrix composites have been fabricated by three major routes: the solid-state process, liquid-state process, and transient phase spray deposition process. In the spray deposition process of Al-MMC, commonly used methods include plasma spraying, physical vapor deposition (PVD), high-velocity-oxy-fuel spraying (HVOF), and cold spraying (CS) [8–10]. In recent years, the cold spray process has emerged as a promising technique to synthesize metal matrix coatings due to the inherent advantages such as no oxidation or phase transformation and minimal grain growth without any interfacial reaction with a matrix. These advantages are achieved by low temperature, which is well below the melting temperature of feedstock powder. This process can retain the

solid-state properties of the feedstock powder after the deposition. Hence, it is also referred to as a solid-state coating process [11]. The high impact velocities during the cold spray process result in severe plastic deformation (SPD) of the particles, and these particles exhibit excellent bonding between the interparticle and substrate. The cold spray process can produce dense and thick coatings in the range of micrometers to several millimeters. However, some porosity and low ductility due to cold working are the major drawbacks of CS coatings. The cold spray process's adverse effects are addressed by the heat treatment of the as-sprayed coating [12–15]. After the heat-treatment of CS coatings, the residual stresses are released, inter-splat bonding is improved, hence mechanical and wear properties could be improved.

Hard nanoparticle reinforced metal matrix coatings have been widely studied due to their excellent mechanical and tribological properties. For the Al-MMC cold spray coatings, the most commonly used hard particle reinforcements are B₄C, SiC, TiN, Al₂O₃, and cBN [16–20]. In recent years, considerable interest in exploring hard nanodiamond (ND) particles has increased because of their excellent thermal conductivity, superior hardness, electrical properties, low coefficient of

* Corresponding author.

E-mail address: agarwala@fiu.edu (A. Agarwal).

friction, improved wear resistance, and chemical stability [21–25]. Nanodiamond (ND) particles have been used as reinforcements and have shown excellent improvement in the mechanical-tribological properties of MMCs [26–29]. Woo et al. have studied cold spray ND reinforced Al-MMC coatings [27,28]. Both these studies' major focus was varying the ND concentration and ball milling duration to synthesize Al-ND MMC's. Stearic acid (3 wt%) was used as a process control agent in both studies to prevent agglomeration [27,28]. ND and Al were mixed uniformly by high-energy mechanical alloying techniques for various milling conditions [27]. 10 wt% ND-Al composite was optimal as it showed a 210% increase in the hardness compared to pure Al. In the next phase, Woo et al. studied the effect of ball milling conditions on the deposition efficiency and mechanical properties of cold-sprayed Al-10 wt% ND coating [28]. Al-ND MMC showed the highest deposition efficiency of 14.2% for 30-minute milled powder feedstock. Significant improvement in hardness (200%) and elastic modulus (51%) of as-sprayed ND reinforced Al-MMC coating was achieved for a 3 h milled sample. Hence, previous studies have successfully demonstrated the feasibility of depositing Al-ND MMC coatings by the cold spray process. However, both the studies displayed carbonaceous residue in the Al-ND MMC's due to the PCA stearic acid thermal decomposition and the formation of Al_4C_3 on the ND surface [27,28]. In the present study, we have deposited Al-ND coatings at a low (2 wt%) concentration of reinforcement without any process control agent. Considering the cost, agglomeration factor, and super abrasive nature of ND (the high concentration of ND can scratch and damage the cold spray equipment during deposition), so a low concentration of reinforcement is chosen in this study. Extensive TEM microstructural characterization of the cold sprayed composite coating has been carried to study ND dispersion. The as-sprayed Al-2 wt % ND coating is heat-treated below the crystallization temperature. The changes in mechanical and tribological properties of the Al-2 wt% ND coating due to heat-treatment are investigated. The observed properties have been elucidated in sub-structure, ND dispersion, and dislocations observed via TEM.

2. Experimental procedure

2.1. Powder feedstock

Aluminum (Al) powder of type H3 was purchased from Valimet Inc. (Stockton, CA, USA). Spherical morphology was chosen for the feedstock powder due to excellent flowability during the cold spray process [30,31]. The as-received Al powder purity was 99.7%, and the particle size varied from 2 to 10.5 μm (Fig. 1(a)). Nanodiamond powder (ND, 98% pure, 3.22 g/cm³) was procured from Nanostructured and Amorphous Materials Inc. (Houston, TX). The particle size varied from 6 to 15 nm, as shown in Fig. 1(b). TEM micrograph inset reveals the spherical nature of the as-received nanodiamond powder.

2.2. Composite powder preparation and cold spray deposition

The metal matrix composite feedstock powder for cold spray deposition was synthesized by ball milling aluminum and nanodiamond powders at room temperature conditions using a ball mill from Across International LLC. Livingston, NJ, USA. The Al and ND powders were subjected to milling for 1 h using stainless steel balls (10 mm diameter) and vial, with a ball to powder ratio of 10:1. Cold spraying deposition was carried out at ASB industries, OH. The AISI 1020 type plain carbon steel substrate with 100 mm × 19 mm × 3 mm was grit blasted to remove the impurities and increase the substrate's surface roughness. This, in turn, enhances the adhesion of the composite coating to the substrate during deposition [32]. Al-2 wt% ND feedstock powder was mixed with preheated N₂ gas at ~673 K and sprayed on the grit blasted substrate kept at ~323 K. During the deposition, the gas pressure and temperature were monitored using the diagnostic ports inside the spray gun. The powder was sprayed onto the substrate at a pressure of 3.8

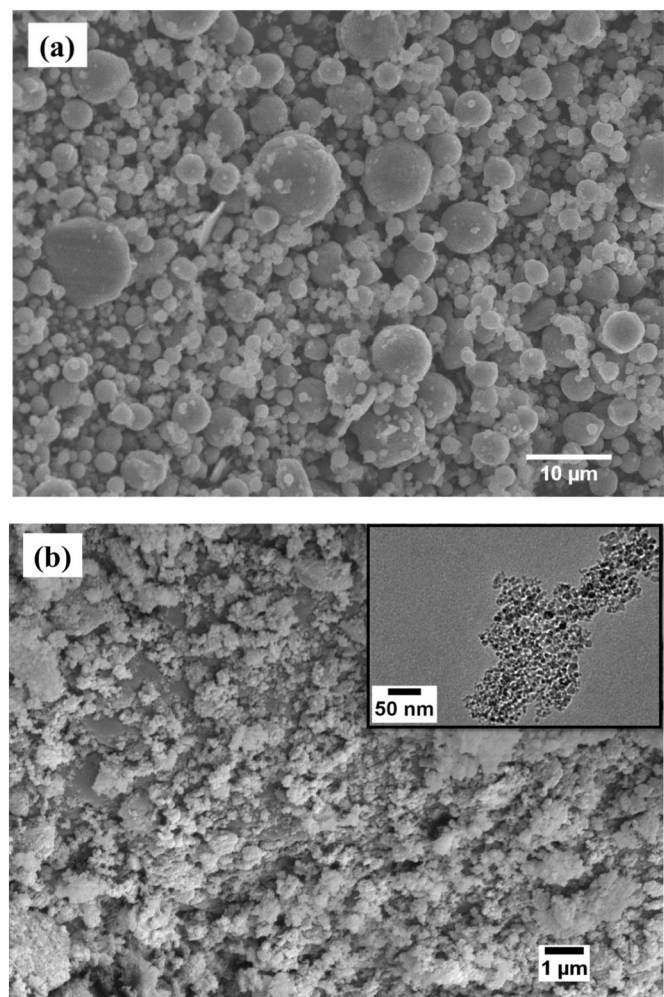


Fig. 1. SEM micrographs of the as-received (a) aluminum and (b) nanodiamond powder with TEM (inset).

MPa, and the stand-off distance was 40 mm. As-sprayed Al-2 wt% ND coating was annealed at 550 °C for 2 h in argon atmosphere, and the sample was subjected to furnace cooling. This heat-treatment is expected to improve the cold-sprayed coating's inter-splat bonding, coating density, and mechanical properties [12,13]. Cold-spray deposition of pure Al coating on plain carbon steel substrate was prepared as the control sample and heat-treated under similar conditions. The influence of heat-treatment on the coating density, phases, microstructure, microhardness, and wear properties was examined.

2.3. Structural and microstructural characterization

Phase analysis of the as-sprayed and heat-treated Al-2 wt% ND coatings were carried out using X-ray diffraction (XRD, Siemens D-5000, Munich, Germany). Microstructural characterization of the feedstock powder, ball-milled powder, and the coating was examined using a scanning electron microscope (SEM, JEOL JSM 6300). The coating cross-sections were characterized by segmenting the samples using a low-speed diamond saw. Further, the samples were mounted in resin and polished up to 0.1 μm finish using alumina suspensions. The polished cross-sections were etched for 5 to 10 s using Keller's reagent. The coating density was measured by processing the cross-sectional micrographs using ImageJ software. The as-sprayed and heat-treated coatings were sectioned from the substrate, and the sectioned coatings were fractured manually under tension. The fractured surface of the coatings was observed under SEM to understand nanodiamond distribution and

splat morphology. Vickers Microhardness was measured in the polished cross-section of the coatings with Type M high-precession Microhardness Tester (Shimadzu, Japan) at a load of 50 g and dwell time of 15 s. A minimum of 5–6 indents was made on the coating cross-section. The distance between each indentation was maintained at least five times the diagonal indent length. For transmission electron microscopy (TEM) study, the sample from the as-sprayed coating cross-section was prepared using a focused ion beam (FIB) milling in SEM (JEOL-JIB 4500). The sample was analyzed using the Philips CM transmission electron microscope operating at 200 kV to study the interface, defects, and nanodiamond dispersion in the matrix.

2.4. Tribological studies

The wear behavior of cold sprayed Al-ND coatings was studied using Nanovea ball-on disk tribometer (Irvine, CA). An alumina (Al_2O_3) ball of 3 mm diameter was used as a counter material. The wear tests were carried out at a normal load of 1 N for a 4 mm diameter circular track at a speed of 10 RPM for 15 min. A minimum of three wear tests was performed at room temperature on the as-sprayed and heat-treated coatings. The COF was measured continuously during the wear tests. After the test, wear track profiles were imaged by a non-contact optical profilometer (PS50, Nanovea, Irvine, CA). The wear depth was obtained by creating 3D profiles of the track using Scanning Probe Image Processor software (SPIP, Image Metrology, Denmark). A minimum of 5 locations was used along the wear track to obtain the depth, and wear track depth profiles were integrated using Origin to compute the wear track's average cross-sectional area. Wear volume loss was calculated by multiplying the average cross-sectional area and circumference of the wear track. Microstructural investigation of the worn surfaces was performed using SEM to understand the wear mechanisms.

3. Results and discussion

3.1. Powder characterization

The feedstock powder for cold spray deposition was processed by ball milling Al and 2 wt% nanodiamond powder for 1 h. This resulted in an excellent distribution of ND in the aluminum matrix. Fig. 2 shows the SEM microstructure of the ball-milled composite powders. The nanodiamond particles were homogeneously mixed and adhered to Al powder's surface, as shown in Fig. 2(b). After milling, no deformation of ND particles was observed. Spherical Al powder shows a change in the particle morphology and size as they become more oblate after ball milling due to plastic deformation. During milling, ductile Al particles collide, fracture, and then the deformed particles cold-weld [33], resulting in the increase of average particle size from 5 μm (as-received Al powder) to 24 μm . A few ND particles could be trapped between the cold-welded Al particles, as schematically shown in Fig. 3. Superhard ND particles distributed within the soft Al matrix would strengthen the metal matrix composite [34,35].

3.2. Phase analysis and microstructure of Al-2 wt% ND coating

Phase analysis using X-ray diffraction (XRD) was performed on the as-sprayed and heat-treated Al-2 wt% ND coatings, as shown in Fig. 4. The predominant phase detected in the as-sprayed and heat-treated Al-2 wt% ND coatings were mainly pure Al with no evidence of any oxide phase. The cubic diamond phase corresponding to nanodiamond was not detected, as the ND concentration was lower than XRD's detection limit. The XRD patterns do not show any carbide (Al_4C_3) phase formation, unlike previous studies that reported Al_4C_3 formation after milling and deposition [27,28]. Lack of Al_4C_3 formation is confirmed by the absence of 2 θ peaks at $\sim 31.5^\circ$ and 55° . As the ND outer surface graphitization was averted by shorter milling duration and lower annealing temperature, it eventually prevents the carbide formation in the feedstock

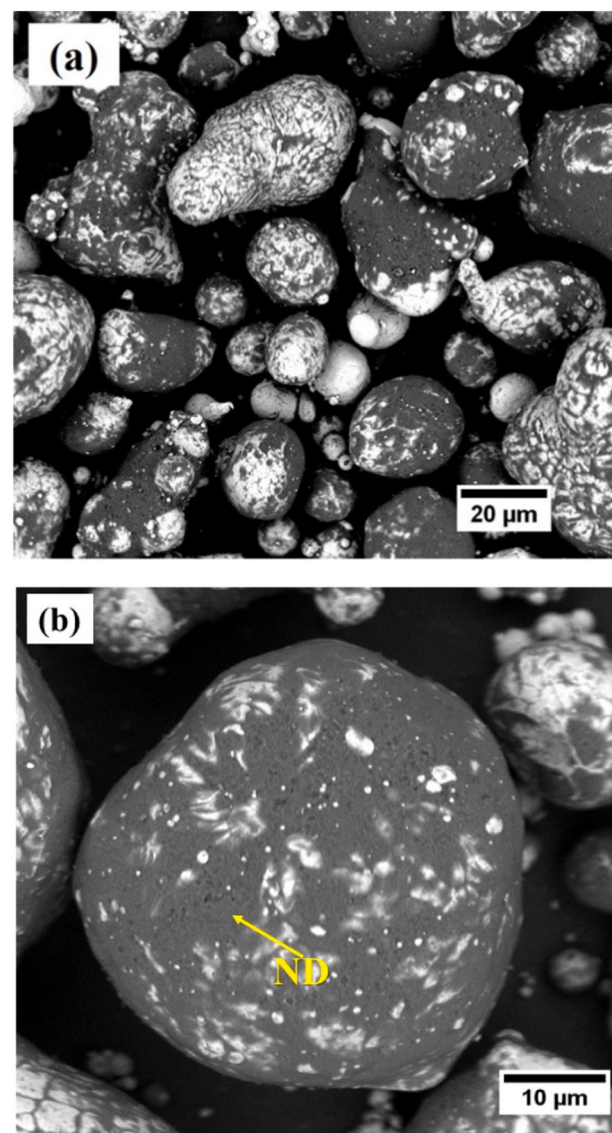


Fig. 2. SEM images of ball-milled Al-2 wt% ND powder at (a) low magnification and (b) high magnification, where the aluminum particles are enveloped with ND powder (low Z-contrast).

powder and coating [27,28,36]. Comparing the 20 peak around $\sim 38.5^\circ$ of as-sprayed and heat-treated condition (Fig. 4), no significant change in FWHM of as-sprayed ($\sim 0.2016^\circ$) and heat-treated condition ($\sim 0.2020^\circ$) was observed. Hence, there was no grain growth seen after the heat-treatment of Al-2 wt% ND coating, indicating the diffusion of nanodiamond from the matrix to the grain boundary upon heat-treatment, which potentially inhibits the grain growth. This grain size retention of heat-treated Al-2 wt% ND coating would effectively contribute to improving its mechanical properties.

The polished cross-section microstructure of as-sprayed and heat-treated Al-2 wt% ND coating was studied using SEM, as shown in Fig. 5. The As-sprayed Al-2 wt% ND coating thickness was $\sim 125 \mu\text{m}$. No imperfections such as delamination/cracking were observed between the coating and substrate interface, indicating excellent interfacial bonding. The as-sprayed coating has fine pores, micro-cracks within individual splats, and inter-splat voids, as shown in the inset of Fig. 5(a). The measured density (ImageJ) of the as-sprayed Al-2 wt% ND coating was 98%. The dense coating was formed with the deposition of thin splats' layers, as shown in Fig. 5(a). The elongated splats were 45 μm long and 0.5–1 μm thick, showing significant plastic strain experienced

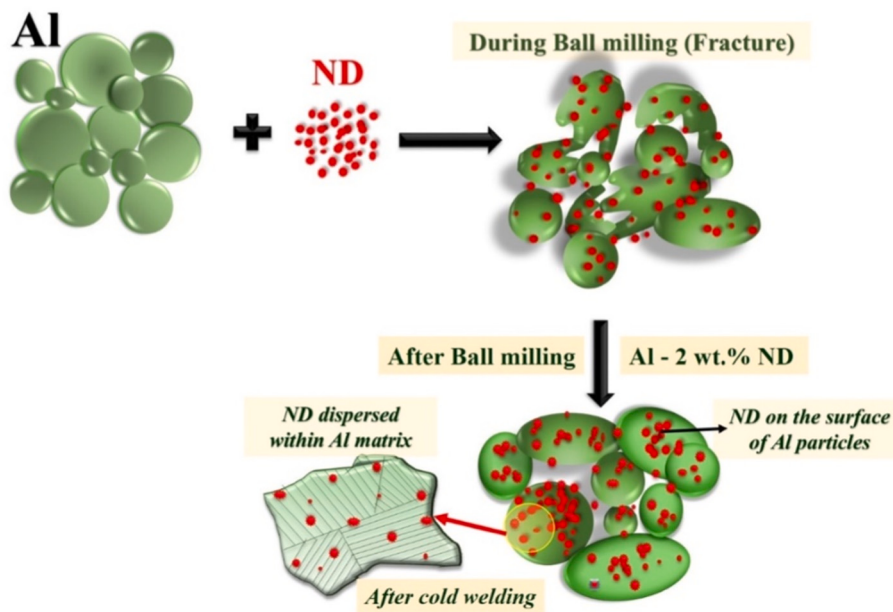


Fig. 3. Schematic representation of various stages of mixing Al-2 wt% ND powder.

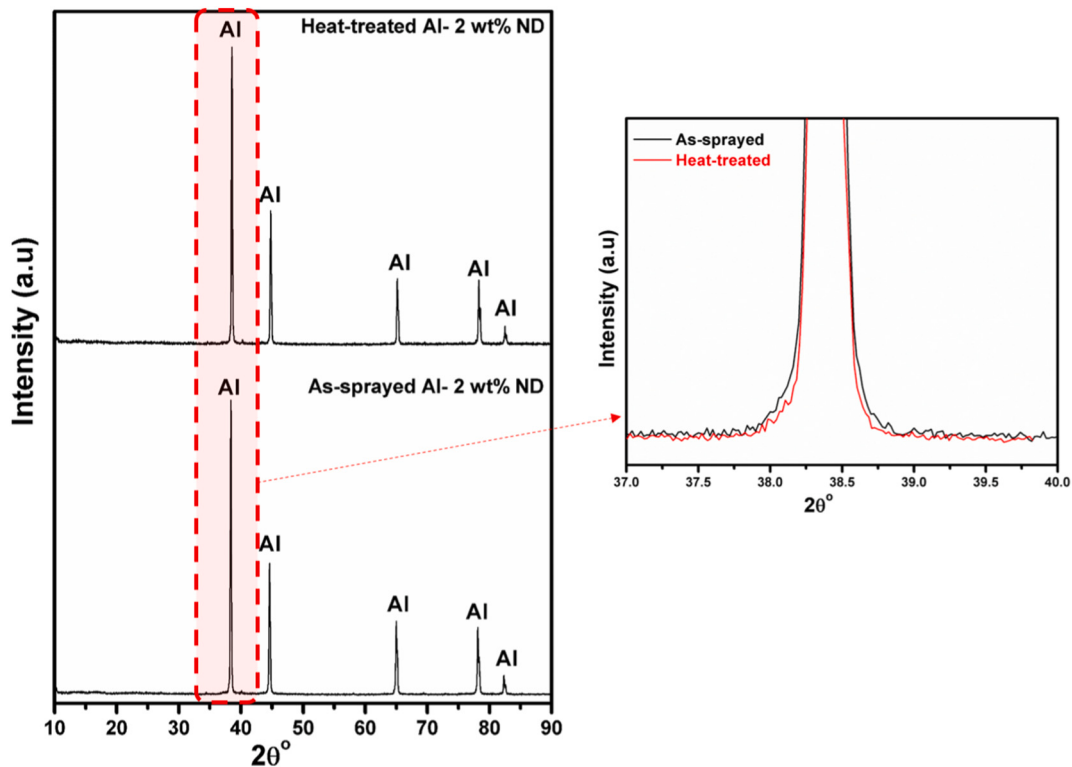


Fig. 4. XRD patterns of the as-sprayed and heat-treated Al-2 wt% ND coating.

by the feedstock particle during deposition. Plastic strain (ϵ_p) is estimated from the particle flattening and is directly related to flow stress (σ) based on the power-law relationship,

$$\sigma = K \epsilon_p^n \quad (1)$$

where K is the material strength coefficient, and n is the material strain, hardening exponent. The above relation indicates aluminum particles were subjected to extensive plastic deformation resulting from high-speed particle impingement during the cold spray process [37].

Fig. 5(b) shows the polished cross-section of heat-treated Al-2 wt% ND coating. Most of the porosity and fine cracks were eliminated post-annealing, and coating density increased to 99%. Also, the interface between the particles could coalesce and trap ND particles inside the splats. This could occur as the ND particles dispersed inside the deformed Al particles with some ND present along the interparticle boundaries during the cold-spray process. Upon heat-treatment, the interface with pores or voids between the deformed particles could coalesce along with good interparticle bonding. In this process, ND

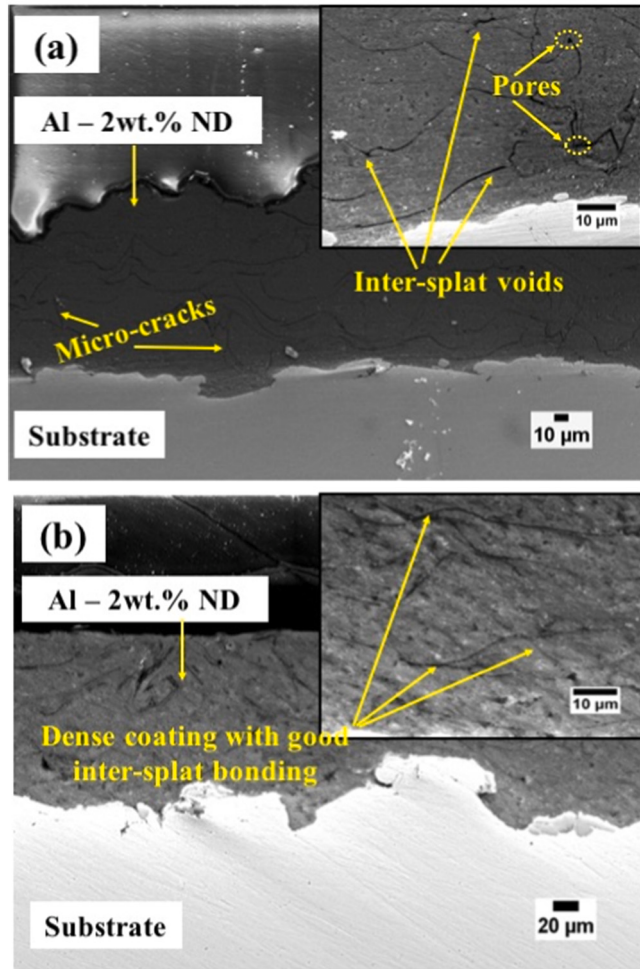


Fig. 5. SEM images of the polished cross-section of (a) as-sprayed and (b) heat-treated Al-2 wt% ND coating.

particles present between the interparticle boundaries could be trapped due to the interparticle/intersplat diffusion. Previous studies on MMC cold spray coatings have observed reinforced particles' presence between the splat boundaries [14,38,39]. Internal stress will be reduced during the heat-treatment of Al-2 wt% ND coating.

Fracture surfaces of Al-2 wt% ND coatings were investigated to understand the inter-particle bonding in the as-sprayed and heat-treated conditions. As-sprayed coating is quite dense, but weak bonding between the splats was observed, resulting in the inter-splat void formation, as shown in Fig. 6(a). Also, crack propagation was transgranular for the as-sprayed coating, where the micro-cracks propagated along the thickness of individual splats and fine pores were observed. During fracture, some of the particles were pulled out from the splats implying the insufficient bonding between the splats. In contrast, the fracture surface of heat-treated Al-2 wt% ND coating showed distinct features from the as-sprayed coating, as shown in Fig. 6(b). Porosity between the splats was mostly eliminated, and comparatively, the dense coating was achieved after heat-treatment. This indicates the stronger bonding between the splats by diffusion in addition to mechanical interlocking. Inter-splat voids were reduced with a decrease in crack nucleation sites after heat-treatment. Several dimples were observed in the fracture region of the heat-treated coating due to micro-void coalescence rupture [40]. It is clear from these dimpled features in the fracture surface; coating ductility has improved post-heat-treatment.

The bright-field TEM image shows an excellent dispersion of ND within the aluminum matrix. The size of ND particles varied from 5 to 15 nm, as shown in Fig. 7(a). As-received nanodiamond particle size was

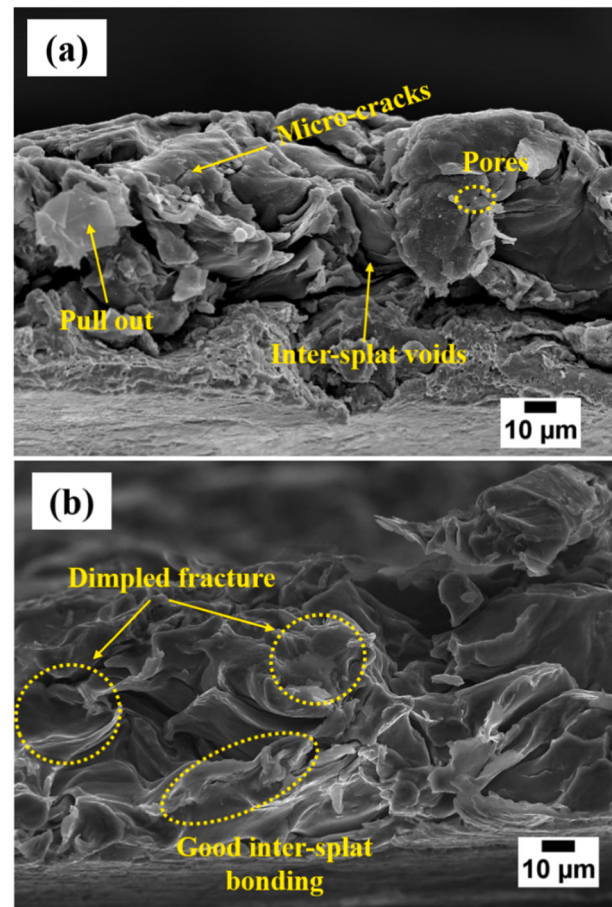


Fig. 6. Fracture surface of (a) as-sprayed and (b) heat-treated the Al-2 wt% ND coating.

retained in the coating without any agglomeration. Most nanodiamonds were distributed within the grains and a few along the grain boundaries (GB). High-resolution TEM (HRTEM) images corresponding to the nanodiamond are shown in Fig. 7(b). The dark spot's lattice spacing is 2.06 Å and conforms to its (111) plane. HRTEM images corroborate nanodiamond's structural and phase purity with a uniform dispersion in the aluminum matrix. Fig. 7(c) represents another TEM image of as-sprayed condition, grain was elongated, and multiple high angle grain boundaries were observed [12]. The elongated grains were developed by high impact pressure during the deposition, resulting in extensive plastic deformation of powder particles. Pile-up of dislocations was observed along the edge of some grains, indicating the severe plastic deformation and accumulation of internal stress during the cold spray process [41,42]. Fig. 8 shows a bright-field TEM image and corresponding selected area electron diffraction (SAED) pattern from the as-sprayed Al-2 wt% ND coating. SAED pattern displays a combination of two different diffraction patterns. The continuous diffraction ring corresponds to the nanodiamond, and the highly intense spot pattern corresponds to Aluminum. This SAED pattern confirms the polycrystalline nature of Aluminum in the as-sprayed coating. Also, contrast inside grains was not uniform and elongation of diffraction spots was observed (Fig. 8). This confirms the development of internal stress and distortion of crystal lattice during Al-2 wt% ND deposition. Fig. 9(a) shows an amorphous region of 10–15 nm thickness formed at the interface between two grains [43,30]. This amorphous zone between grain boundaries could be created by particle impact during the cold-spray process. These impacts induce severe plastic deformation between particles, which results in melting at the particle interfaces, and further quenching it rapidly promotes the amorphous layer formation. HRTEM image in

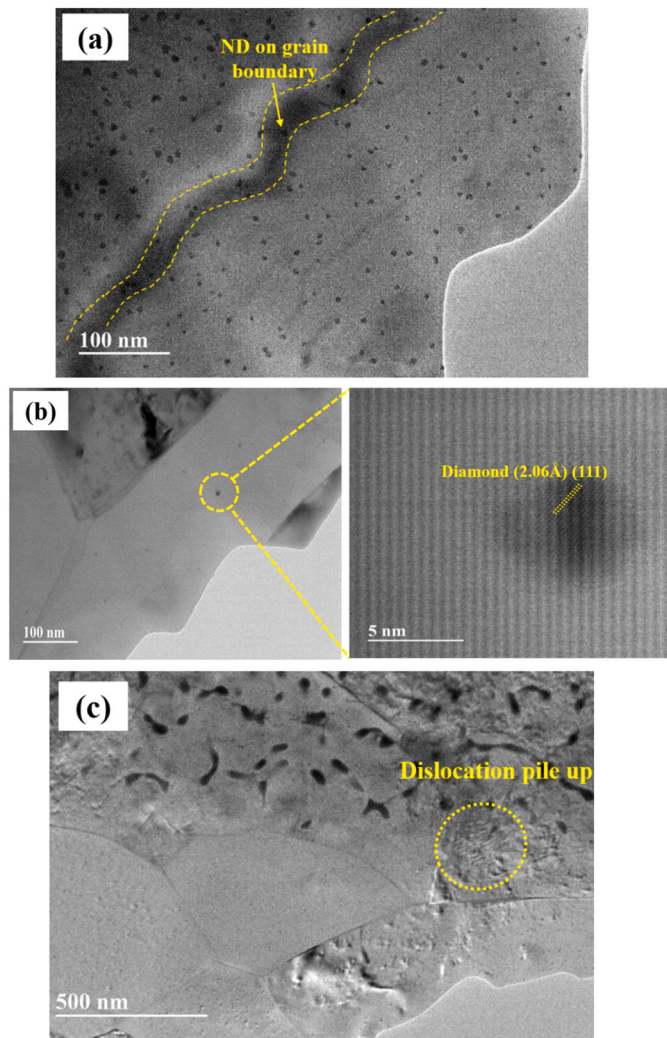


Fig. 7. (a) Bright-field TEM image showing the excellent dispersion of ND in the cold sprayed Al-2 wt% ND coating, (b) HRTEM image of cold sprayed coating showing the ND inside the aluminum matrix, and (c) bright-field TEM image of cold sprayed Al-2 wt% ND coating.

Fig. 9(b) shows the pile-up of dislocation in the grain boundaries along the (200) plane. This high level of dislocation along the grain boundary indicates grain boundary regions were heavily deformed with high dislocation densities, and grains inner region were mostly free from dislocations. Non-equilibrium grain boundaries could be formed due to the high dislocations pile-up along the grain boundaries.

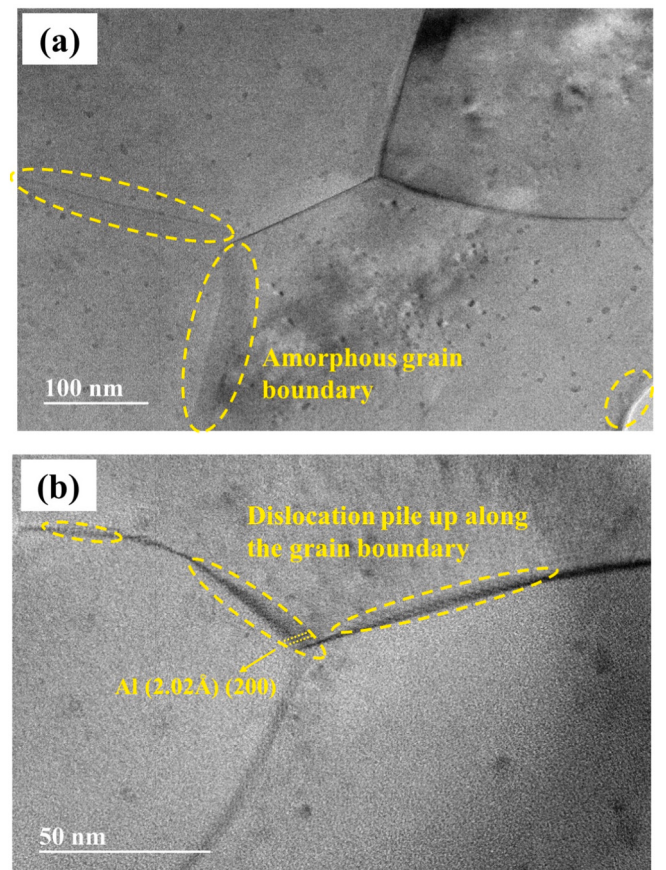


Fig. 9. Bright-field TEM image of cold sprayed Al-2 wt% ND coating showing the presence of (a) amorphous grain boundary and (b) dislocation pile-up along the grain boundary.

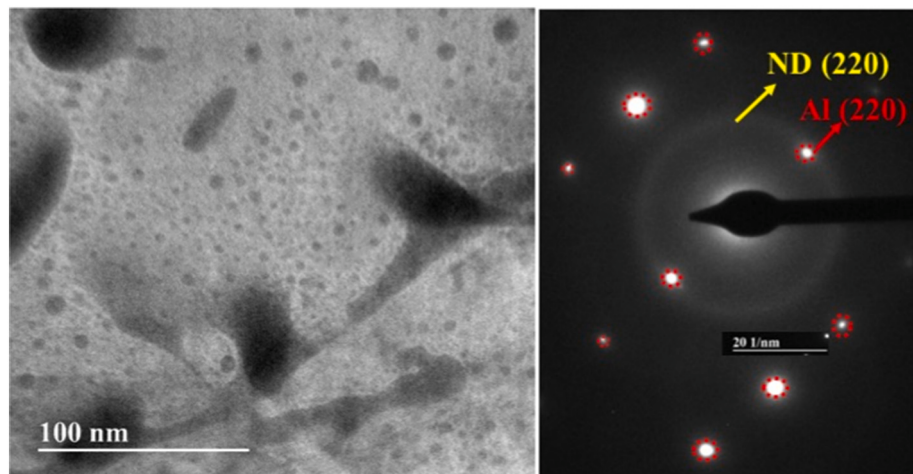


Fig. 8. Bright-field TEM image and corresponding SAED pattern display ring pattern corresponding to ND phase and spotty diffraction pattern belonging to Al phase.

3.3. Microhardness

To understand nanodiamond reinforcement's effect on Al matrix composites' microhardness, measurements from the polished cross-section of cold spray Al and Al-2 wt% ND coatings are shown in Fig. 10. The microhardness of as-sprayed Al (45.1 ± 1.1 HV) coating is comparable to the microhardness of bulk Al (56.2 ± 4 HV) prepared by spark plasma sintering [44]. Microhardness of the cold-sprayed pure Al coating decreased by ~12% after heat-treatment due to the grain coarsening and residual stress release [45,46]. With the addition of nanodiamond, the microhardness of as-sprayed Al-2 wt% ND coating increased to 65.3 ± 2.12 HV, about 96% improvement compared to as-sprayed pure Al coating. The hardness ($H_{CS(Al-ND)}$) increment of as-sprayed Al-2 wt% ND coating compared to pure Al coating can be summarized based on a simple rule of the mixture as below,

$$H_{CS(Al-ND)} = f_{ND}H_{ND} + (1 - f_{ND})H_{CS(Al)} \quad (2)$$

where f_{ND} is the volume fraction of ND, H_{ND} is the hardness of ND, and $H_{CS(Al)}$ is the hardness of cold spray aluminum. The $H_{CS(Al)}$ can be described as below,

$$H_{CS(Al)} = H_{Al} + \Delta H_S + \Delta H_{WH} \quad (3)$$

where H_{Al} is the hardness of Aluminum, ΔH_S is the strengthening due to fine grains size and ΔH_{WH} is the strengthening due to work hardening during the cold spray process. Thus, based on Eqs. (2) and (3), the increase in microhardness of as-sprayed Al-2 wt% ND coating can be demonstrated by (i) hard nanodiamond reinforcement in Al matrix resulting in dispersion strengthening, (ii) fine grain size of Al matrix, and (iii) work hardening of Aluminum during the cold spray process [21,22]. After heat-treatment of Al-2 wt% ND coating, microhardness increased to 153 ± 2.5 HV, which is 135% higher than as-sprayed Al-2 wt% ND coating. This significant improvement after heat-treatment could be attributed to (i) diffusion of ND particles along the grain boundary-inhibits the grain growth and increases the resistance to plastic deformation, (ii) diffusion of dislocations with simultaneous [12] (iii) decrease in coating porosity by improving the bonding between splats [12,13].

3.4. Tribological studies

Friction and wear properties of the as-sprayed and heat-treated Al-2 wt% ND coatings were studied using a ball-on-disk tribometer. The variation in friction (COF) coefficient concerning sliding time for the as-sprayed and heat-treated coatings is shown in Fig. 11. For the as-sprayed

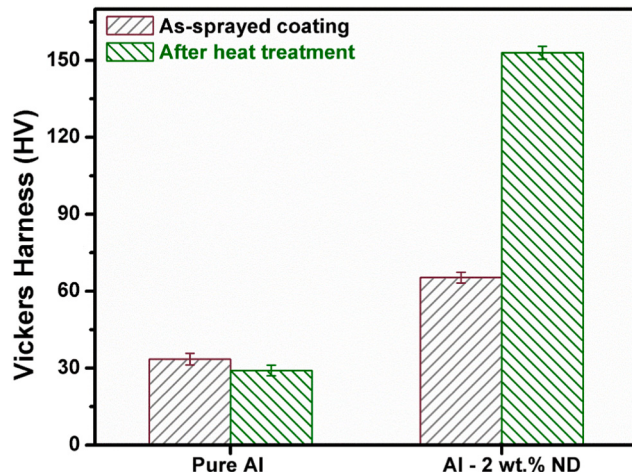


Fig. 10. Microhardness variation of cold-sprayed pure Al and Al-2 wt% ND coating before and after heat-treatment.

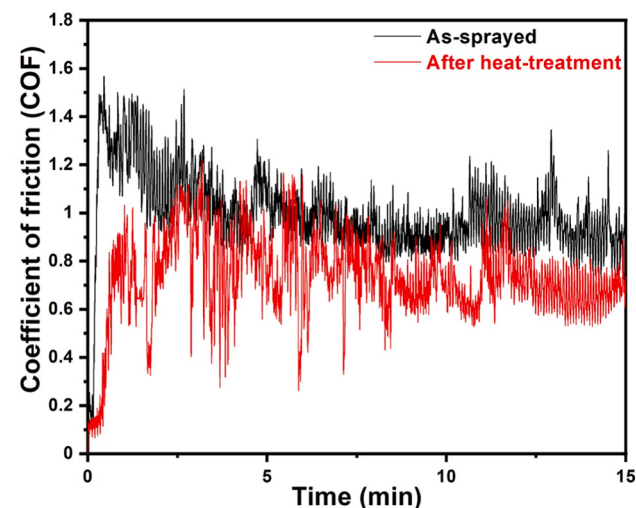


Fig. 11. Coefficient of friction variation for cold-sprayed Al-2 wt% ND coating before and after heat-treatment.

Al-2 wt% ND coating, the measured average COF was $\sim 1.15 \pm 0.013$. Initially, a higher COF value (1.2–1.4) was seen for the first 3 min, and after that, the COF gradually stabilized. The average COF was $\sim 0.74 \pm 0.021$ for the heat-treated Al-2 wt% ND coating. The large fluctuation in the COF (0.4–1.1) was observed for the first 8 min, and then it drops to ~ 0.7 . The heat-treated coatings COF was about $\sim 35\%$ lower than the as-sprayed coating.

From the 3D optical profiles of wear tracks, wear depth of as-sprayed and heat-treated Al-2 wt% ND coatings were measured. Fig. 12 shows the wear depth of 50 μm for the as-sprayed wear track, and after heat-treatment, it dropped to 40 μm . The wear depth of the heat-treated coating decreased by $\sim 20\%$ compared to the as-sprayed coating, indicating the improved wear properties after heat-treatment. The cross-sectional area of the wear track was computed using wear depth. Wear volume loss of wear track was calculated for both the conditions by multiplying cross-sectional area and circumference of wear track. The average wear volume loss of as-sprayed and heat-treated coating was $0.29 \pm 0.02 \text{ mm}^3$ and $0.18 \pm 0.002 \text{ mm}^3$, respectively. After heat-treatment of Al-2 wt% ND coating, wear volume loss was decreased by $\sim 38\%$. Based on Archard's law, the wear rate (k , $\text{mm}^3/\text{N mm}$) is measured by,

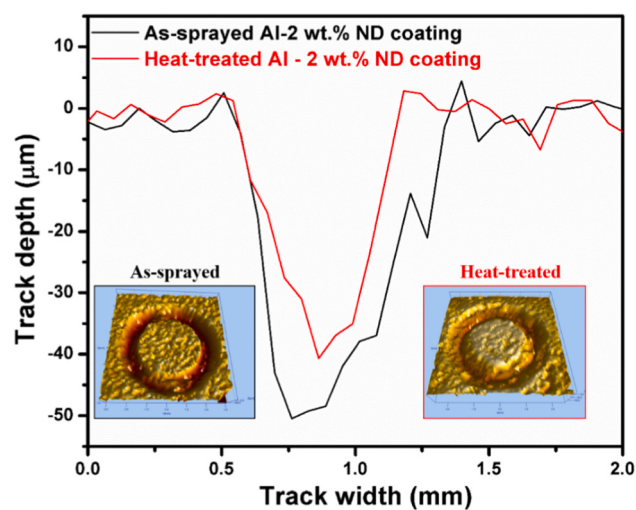


Fig. 12. Wear track depth 2D line profile of cold-sprayed Al-2 wt% ND coating before and after heat-treatment.

$$k = \frac{V}{P \times S} \quad (4)$$

where V - wear volume loss (mm^3), P - applied load (N), S - sliding distance (mm). Using Eq. (4), the measured wear rate for as-sprayed and the heat-treated coating is $1.48 \pm 0.121 \times 10^{-4} \text{ mm}^3/\text{N mm}$ and $0.975 \pm 0.075 \times 10^{-4} \text{ mm}^3/\text{N mm}$, respectively. Compared to the as-sprayed condition, the wear rate was reduced by 35% for the heat-treated coating.

To understand the wear mechanism for as-sprayed and heat-treated Al-2 wt% ND coating, wear track surfaces were observed under SEM. Low magnification images of wear track surface for both conditions are shown in Fig. 13(a) and (c). High magnification images of the wear track surface for both conditions are shown in Fig. 13(b) and (d). SEM image in Fig. 13(a) represents the worn surface of as-sprayed Al-2 wt% ND coating, exhibiting severe wear with a rough surface and parallel grooves/scratches formed along the sliding direction. The groove formation contributes from the loosely adhered hard nanodiamond particles between the splats, resulting in third-body abrasion. In addition, significant delamination with material loss was observed in Fig. 13(a). Fine pores between the splats along with micro-cracks formed on the wear surface were visible at higher magnification (Fig. 13(b)). The pre-cracks in the as-sprayed coating were generated due to weak bonding between splats. During sliding wear, pre-cracks grow to form micro-cracks along the wear track. High magnification SEM images reveal continuous and deep grooves with delamination, resulting in a higher wear rate of as-sprayed coatings. This could be the result of nanodiamond retention with no surface graphitization as the nanodiamond observed in the as-sprayed coating TEM image (Fig. 7(b)) point to the absence of graphitic layers around the ND, and the observed lattice spacing (2.06 \AA) matches with diamond (111) plane. Wear track surface indicates that the dominant mechanism for as-sprayed Al-2 wt% ND coating is through abrasive wear, which is schematically depicted in Fig. 14(a). This results in poor friction and wear properties of as-sprayed

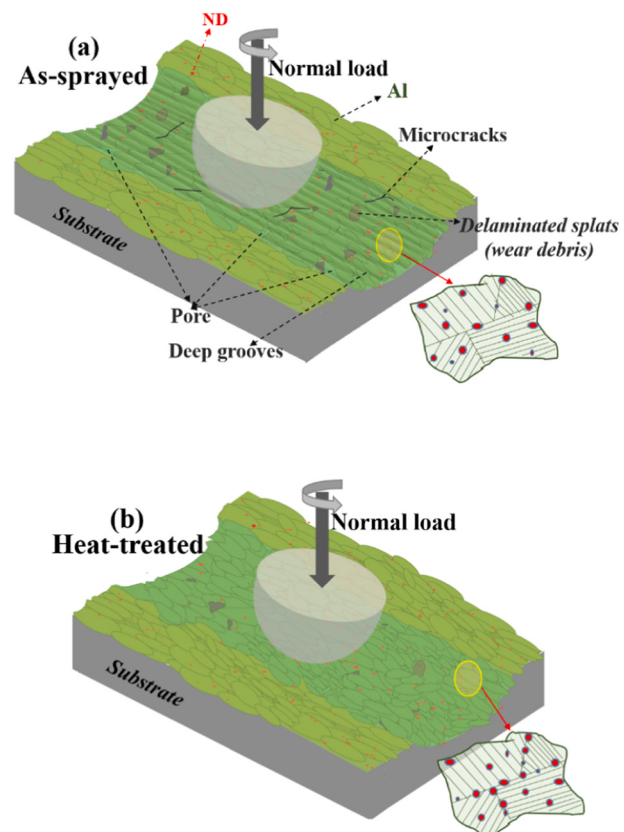


Fig. 14. Schematic diagram of wear mechanism of Al-2 wt% ND coating in the (a) as-sprayed and (b) heat-treated condition.

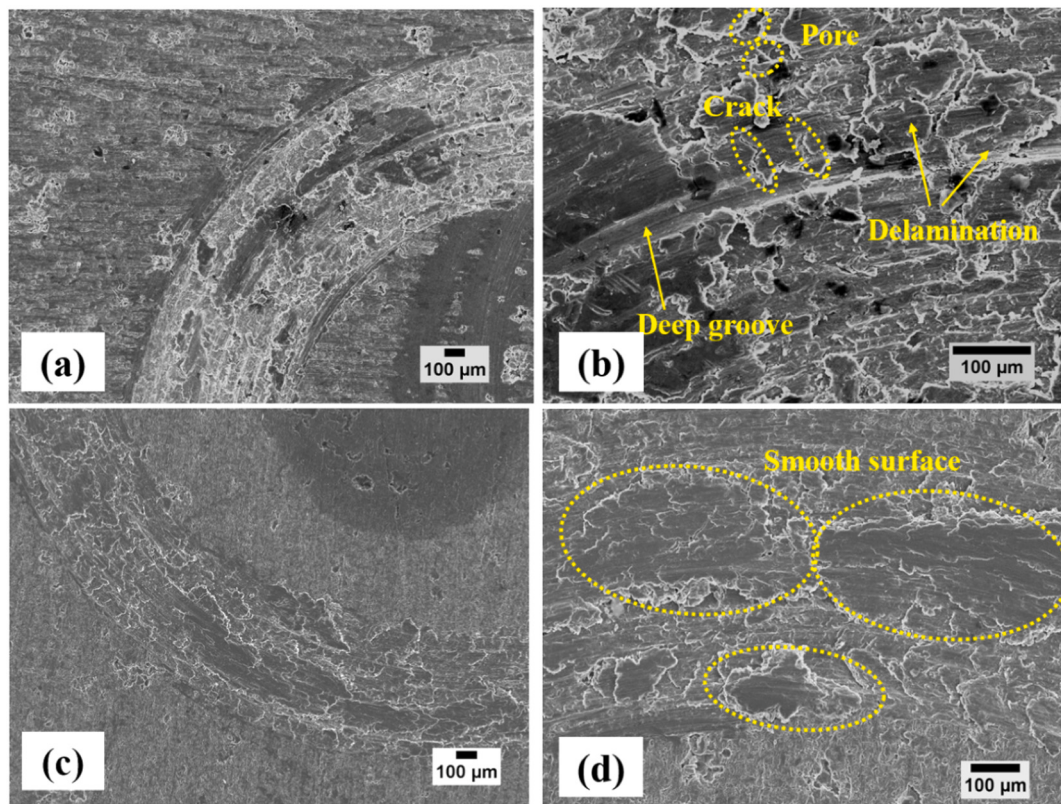


Fig. 13. SEM images of wear track (a, b) as-sprayed and (c, d) heat-treated Al-2 wt% ND coating.

Al-2 wt% ND coating regardless of uniform distribution of nanodiamond in the matrix. Heat-treated Al-2 wt% ND coating wear track surface exhibited partial plastic deformation of splats, as shown in Fig. 13(c). The smooth and clean wear track surface was displayed at a higher magnification SEM image (Fig. 13(d)). No cracking or pore was observed on the wear track surface of heat-treated Al-2 wt% ND coating, suggesting good intersplat bonding and uniform nanodiamond dispersion, thus improving the wear resistance of heat-treated coating as displayed in heat-treated wear model schematic (Fig. 14(b)). Some of the nanodiamonds trapped between the splats upon heat-treatment would have undergone partial graphitization - forming an sp^2 -carbon layer on the surface of ND, as previously observed by Cebik et al., in the heat-treatment of ND powders in an inert environment lead to the sp^3 -to- sp^2 conversion of the surface, beginning with smaller ND crystals at temperatures as low as 600–700 °C [36]. This layered sp^2 -carbon during the wear test resulted in smooth wear track surface for the heat-treated coating. Hence, a reduction in friction and wear rate of heat-treated coating is ascribed to increased density, high hardness, fine grain structure, and ND surface graphitization during the wear test.

4. Conclusion

The cold spray process successfully fabricated a low concentration nanodiamond reinforced aluminum matrix (Al-2 wt% ND) composite coating. The influence of heat-treatment in microstructure, mechanical, and tribological properties has been studied. The key findings of this study are as follows:

- X-ray diffraction study of heat-treated Al-2 wt% ND coating revealed no phase transformation and grain growth. The nanodiamond presence restrained the grain growth upon heat-treatment and retained the fine microstructures. Dimpled fracture and good intersplat bonding of Al-2 wt% ND coating was observed post-heat-treatment.
- TEM of as-sprayed coating exhibited an excellent distribution of nanodiamond in the matrix, dislocation pile-up along the grain boundary, and edges of grain.
- Microhardness increased two-fold for heat-treated Al-2 wt% ND coating. This is correlated to ND and dislocations diffusion along the grain boundary with improved bonding between splats.
- Post-heat-treatment, the friction and wear rate coefficient decreased by 35% for the Al-2 wt% ND coating is attributed to the high hardness, improved coating density, ductile nature of the heat-treated coating, and surface graphitization of ND.
- Low concentration of ND (2 wt%) averted agglomeration with a uniform dispersion of ND in the Al matrix and significantly enhanced mechanical properties.

This study suggests that nanodiamond reinforced aluminum matrix cold spray coating with heat-treatment has significant potential as a wear-resistant coating.

CRediT authorship contribution statement

Archana Loganathan: conducted wear and SEM experiments and wrote the manuscript
 Sara Rengifo: conducted powder preparation and microscopic analysis on coatings
 Alex Franco: conducted TEM investigation
 Cheng Zhang: powder preparation and wear experiments supervision
 Arvind Agarwal: conceptualization, writing - reviewing and editing.

Declaration of competing interest

The authors declare that they have no known competing financial interests or personal relationships that could have appeared to influence the work reported in this paper.

Acknowledgments

The authors thank the Advanced Materials Engineering Research Institute (AMERI) at Florida International University for the characterization facilities.

References

- [1] D.B. Miracle, Metal matrix composites – from science to technological significance, Compos. Sci. Technol. 65 (2005) 2526–2540.
- [2] A. Mortensen, J. Llorca, Metal matrix composites, Annu. Rev. Mater. Res. 40 (2010) 243–270.
- [3] N. Chawla, K.K. Chawla, Metal Matrix Composites, Springer, 2006.
- [4] R. Schaller, Metal matrix composites, a smart choice for high damping materials, J. Alloys Compd. 355 (2003) 131–135.
- [5] J.R. Davis, ASM Specialty Handbook: Aluminum and Aluminum Alloys, ASM International, 1993.
- [6] F.S.D. Silva, J. Bedoya, S. Dosta, N. Cinca, I.G. Cano, J.M. Guilemany, A. V. Benedetti, Corrosion characteristics of cold gas spray coatings of reinforced aluminum deposited onto carbon steel, Corros. Sci. 114 (2017) 57–71.
- [7] W.S. Miller, L. Zhuang, J. Bottema, A.J. Wittebrood, P. De Smet, A. Haszler, A. Vieregg, Recent development in aluminum alloys for the automotive industry, Mater. Sci. Eng. A 280 (2000) 37–49.
- [8] S.R. Bakshi, V. Singh, S. Seal, A. Agarwal, Aluminum composite reinforced with multiwalled carbon nanotubes from plasma spraying of spray dried powders, Surf. Coat. Technol. 203 (2009) 1544–1554.
- [9] J.A. Picas, A. Forn, R. Rilla, E. Martin, HVOF thermal sprayed coatings on aluminum alloys and aluminum matrix composites, Surf. Coat. Technol. 200 (2005) 1178–1181.
- [10] E. Sansoucy, P. Marcoux, L. Ajdelstajn, B. Jodoin, Properties of SiC-reinforced aluminum alloy coatings produced by the cold gas dynamic spraying process, Surf. Coat. Technol. 202 (2008) 3988–3996.
- [11] A. Moridi, S.M. Hassani-Gangaraj, M. Guagliano, M. Dao, Cold spray coating: a review of material systems and future perspectives, Surf. Eng. 30 (2014) 369–395.
- [12] M.R. Rokni, C.A. Widener, V.K. Champagne, G.A. Crawford, S.R. Nutt, The effects of heat treatment on 7075 Al cold spray deposits, Surf. Coat. Technol. 310 (2017) 278–285.
- [13] R. Huang, M. Sone, W. Ma, H. Fukanuma, The effects of heat treatment on the mechanical properties of cold-sprayed coatings, Surf. Coat. Technol. 261 (2015) 278–288.
- [14] A. Loganathan, S. Rengifo, A.F. Hernandez, Y. Emirov, C. Zhang, B. Boesl, A. Agarwal, Effect of 2D WS₂ addition on the cold-sprayed aluminum coating, J. Therm. Spray Technol. 26 (2017) 1585–1597.
- [15] P. Nautiyal, C. Zhang, V.K. Champagne, B. Boesl, A. Agarwal, In-situ mechanical investigation of the deformation of splat interfaces in cold-sprayed aluminum alloy, Mater. Sci. Eng. A 737 (2018) 297–309.
- [16] M. Yandouzi, A.J. Bottger, R.W.A. Hendrikx, M. Brochu, P. Richer, A. Charest, B. Jodoin, Microstructure and mechanical properties of B₄C reinforced Al-based matrix composite coatings deposited by CGDS and PGDS processes, Surf. Coat. Technol. 205 (2010) 2234–2246.
- [17] M. Yandouzi, P. Richer, B. Jodoin, SiC particulate reinforced Al-12Si alloy composite coatings produced by the pulsed gas dynamic spray process: microstructure and properties, Surf. Coat. Technol. 203 (2009) 3260–3270.
- [18] M. Yu, W.Y. Li, X.K. Suo, H.L. Liao, Effects of gas temperature and ceramic particle content on microstructure and microhardness of cold sprayed SiCp/Al 5056 composite coatings, Surf. Coat. Technol. 220 (2013) 102–106.
- [19] Q. Wang, N. Birbilis, H. Huang, M.X. Zhang, Microstructure characterization and nano-mechanics of cold-sprayed pure Al-Al₂O₃ composite coatings, Surf. Coat. Technol. 232 (2013) 216–223.
- [20] X.T. Luo, C.-J. Li, Large sized cubic BN reinforced nanocomposite with improved abrasive wear resistance deposited by cold spray, Mater. Des. 83 (2015) 249–256.
- [21] V.N. Mochalin, O. Shenderova, D. Ho, Y. Gogotsi, The properties and applications of nanodiamonds, Nat. Nanotechnol. 7 (2012) 11–23.
- [22] A.A. Balandin, Thermal properties of graphene and nanostructured carbon materials, Nat. Mater. 10 (2011) 569–581.
- [23] S. Osswald, G. Yushin, V. Mochalin, S.O. Kucheyev, Y. Gogotsi, Control of sp^2 / sp^3 carbon ratio and surface chemistry of nanodiamond powders by selective oxidation in air, J. Am. Chem. Soc. 128 (2006) 11635–11642.
- [24] H. Kwon, G.-G. Lee, S.-G. Kim, B.-W. Lee, W.-C. Seo, Mechanical properties of nanodiamond and multi-walled carbon nanotubes dual-reinforced aluminum matrix composite materials, Mater. Sci. Eng. A 632 (2015) 72–77.
- [25] M. Bao, C. Zhang, D. Lahiri, A. Agarwal, The tribological behavior of plasma-sprayed Al-Si composite coatings reinforced with nanodiamond, Journal of the Minerals, Metals & Materials Society 64 (2012) 702–708.
- [26] V. Livramento, J.B. Correia, N. Shohoji, E. Osawa, Nanodiamond as an effective reinforcing component for nano-copper, Diam. Relat. Mater. 16 (2007) 202–204.
- [27] D.J. Woo, B. Snead, F. Peerally, F.C. Heer, L.N. Brewer, J.P. Hooper, S. Osswald, Synthesis of nanodiamond-reinforced aluminum metal composite powders and coatings using high-energy ball milling and cold spray, Carbon 63 (2013) 404–415.
- [28] D.J. Woo, F.C. Heer, L.N. Brewer, J.P. Hooper, S. Osswald, Synthesis of nanodiamond-reinforced aluminum metal matrix composites using cold-spray deposition, Carbon 86 (2015) 15–25.
- [29] F.M. Zhang, T.F. Liu, Nanodiamonds reinforced titanium matrix nanocomposites with network architecture, Compos. B Eng. 165 (2019) 143–154.

- [30] K. Balani, T. Laha, A. Agarwal, J. Karthikeyan, N. Munroe, Effect of carrier gases on microstructural and electrochemical behavior of cold-sprayed 1100 aluminum coating, *Surf. Coat. Technol.* 95 (2005) 272–279.
- [31] W. Wong, P. Vo, E. Irissou, A.N. Ryabinin, J.G. Legoux, S. Yue, Effect of particle morphology and size distribution on cold-sprayed pure titanium coatings, *J. Therm. Spray Technol.* 22 (2013) 1140–1153.
- [32] S. Theimer, M. Graunitz, M. Schulze, F. Gaettner, T. Klassen, Optimization adhesion in cold spraying onto hard substrates: a case study for brass coatings, *J. Therm. Spray Tech.* 28 (2019) 124–134.
- [33] P.R. Soni, Mechanical Alloying: Fundamentals and Applications, Cambridge International Science Publishing Limited, Cambridge, 2001.
- [34] K. Morsi, A. Esawi, Effect of mechanical alloying time and carbon nanotube (CNT) content on the evolution of aluminum (Al)-CNT composite powders, *J. Mater. Sci.* 42 (2007) 4954–4959.
- [35] D. Sneed, Synthesis and characterization of Al-nanodiamond composite powders by high-energy ball milling, Naval Postgraduate School, 2011. <http://hdl.handle.net/10945/10698>.
- [36] J. Cebik, J. McDonough, F. Peirally, R. Medrano, I. Neitzel, Y. Gogotsi, S. Osswald, Raman spectroscopy of the transformation of detonation nanodiamond to carbon onions during low temperature annealing, *Nanotechnology* 24 (2013), 205703.
- [37] V.K. Champagne, D.J. Helfritch, M.D. Trexler, B.M. Gabrial, The effect of cold spray impact velocity on deposit hardness, *Model. Simul. Mater. Sci. Eng.* 18 (2010) 1–8.
- [38] X. Xie, Y. Ma, C. Chen, G. Ji, C. Verdy, H. Wu, Z. Chen, S. Yuan, B. Normand, S. Yin, Cold spray additive manufacturing of metal matrix composites (MMCs) using a novel nano-TiB₂-reinforced 7075 Al powder, *J. Alloys Compd.* 819 (2020), 152962.
- [39] S.R. Bakshi, V. Singh, K. Balani, D. Graham McCartney, S. Seal, A. Agarwal, Carbon nanotube reinforced aluminum composite coating via cold spraying, *Surf. Coat. Technol.* 202 (2008) 5162–5169.
- [40] G. Bae, S. Kumar, S. Yoon, K. Kang, H. Na, H.J. Kim, C. Lee, Bonding features and associated mechanisms in kinetic sprayed titanium coatings, *Acta Mater.* 57 (2009) 5654–5666.
- [41] J.Y. Huang, Y.T. Zhu, H. Jiang, T.C. Lowe, Microstructures and dislocation configurations in nanostructured Cu processed by repetitive corrugation and straightening, *Acta Mater.* 49 (2001) 1497–1505.
- [42] K. Balani, A. Agarwal, S. Seal, J. Karthikeyan, Transmission electron microscopy of cold sprayed 1100 aluminum coating, *Scripta Mater.* 53 (2005) 845–850.
- [43] K.H. Ko, J.O. Choi, H. Lee, Intermixing and interfacial morphology of cold-sprayed Al coatings on steel, *Mater. Lett.* 136 (2014) 45–47.
- [44] S. Rengifo, A comparison between graphene and WS₂ as solid lubricant additives to aluminum for automobile applications, (2015). FIU Electronic Theses and Dissertations. 1862. <https://digitalcommons.fiu.edu/etd/1862>.
- [45] H.Y. Bu, M. Yandouzi, C. Lu, B. Jodoin, Post-heat treatment effects on cold-sprayed aluminum coatings on AZ91D magnesium substrates, *J. Therm. Spray Technol.* 21 (2012) 731–739.
- [46] K.S. Al-Hamdan, J.W. Murray, T. Hussain, A.T. Clare, Heat-treatment and mechanical properties of cold-sprayed high strength Al alloys from satellite feedstocks, *Surf. Coat. Technol.* 374 (2019) 21–31.